5-2011

A Preliminary Climatology of Tropical Moisture Exports in the Southern Hemisphere

Alicia M. Bentley
University at Albany, State University of New York

Lance F. Bosart
University at Albany, State University of New York

Jason M. Cordeira
University at Albany, State University of New York

A Preliminary Climatology of Tropical Moisture Exports in the Southern Hemisphere

Undergraduate Research, ATM 499 · Fall 2010–Spring 2011
Date: 2 May 2011

ALICIA M. BENTLEY, LANCE F. BOSART, and JASON M. CORDEIRA

Department of Atmospheric and Environmental Sciences

University at Albany, State University of New York, Albany, New York

Abstract

Date: 2 May 2011

Heavy precipitation events in the midlatitudes can be supported by the poleward transport of tropical air masses within the warm sector of extratropical cyclones. Previous studies have established a climatology of the four preferred pathways of tropical moisture export (TME) events into the midlatitudes over the Northern Hemisphere (NH). The present study constructs a similar climatology of TME timing and frequency over the Southern Hemisphere (SH), highlighting three preferential regions for tropical-midlatitude interaction. These regions correspond to the locations of the: (i) South Pacific convergence zone (Pacific Ocean pathway, PO), (ii) South Atlantic convergence zone (South American pathway, SA), and (iii) South Indian convergence zone (Southeast African pathway, SEA).

A Eulerian precipitable water (PW) climatology is constructed to isolate individual TME events within the three preferred pathways in the SH. The climatology identifies PW values along 30°S at 5° increments, extracting values four-times-daily from the 2.5° NCEP-NCAR reanalysis dataset for 1979−2007. Potential TME events are identified when two neighboring grid points have PW values >93rd percentile of their monthly PW distribution for >24 h. Potential events are classified as TMEs following human verification of the event's tropospheric structure.

The present investigation reveals that TME frequency in the SH varies on intraseasonal and interannual timescales. The PO pathway exhibits the least seasonal variability of the three examined locations, while the SEA pathway is over three times as active during the SH meteorological summer (DJF). An in-depth analysis of the overall synoptic/dynamic mechanisms associated with TME events in the SEA pathway is performed in this study, linking the observed DJF peak in TME activity to the to the active phase of the South Indian convergence zone.

1. Introduction

The Earth's atmosphere carries out the majority of its midlatitude meridional water vapor transport in narrow, poleward extending regions located within the warm sector of extratropical cyclones (Browning and Pardoe 1973). More recent studies (e.g., Newell et al. 1992, Zhu and Newell 1994, 1998) determined that >90% of the total midlatitude vertically integrated water vapor flux occurs within thin longitudinal corridors that cover <10% of the Earth's circumference. The long and narrow nature of these features caused the authors to label them atmospheric/tropospheric rivers. Knippertz and Martin (2007) suggested the alternate use of the term "moisture conveyor belts" for these formations to emphasize "the analogy with the well-established conveyor belt model of extratropical cyclones" by Carlson (1980). A subsequent paper by Knippertz and Wernli (2010) refers to the entire group of phenomena as tropical moisture export (TME) events and provides a climatology of the preferred pathways of these features over the Northern Hemispheric (NH) midlatitudes.

Four preferred NH pathways for TMEs were identified in the Knippertz and Wernli (2010) study. The first, and most well-known, is the "Pineapple Express": a corridor that connects tropical moisture near the Hawaiian Islands and the west coast of North America. The second favored region of poleward moisture transport occurs along the east coast of Asia. Labeled the "Western Pacific" pathway, a local peak in tropical moisture transport is observed in the summer months and is likely associated with the East Asian monsoon. The third preferred pathway, the "Gulf Stream," is located in the western North Atlantic. TMEs in this region can contribute to heavy precipitation events along the east coast of the United States and in western

Europe. The fourth, and most longitudinally confined corridor, is the "Great Plains" pathway. Located between the Rocky and Appalachian Mountains, the "Great Plains" pathway has moisture sources in the Gulf of Mexico and Caribbean Sea and is the only preferred continental pathway for tropical moisture transport in the NH.

All four NH pathways occur on the western edge of subtropical high pressure centers, paralleling the poleward redirection of warm ocean currents. The differences in seasonal maxima and minima in TME frequency correspond to intraseasonal variations in the surrounding large scale circulations (e.g., position of subtropical high pressure centers, etc.). The lack of TME activity over Africa/India is likely due to the significant topography of the region which provides a formidable obstacle to poleward flow.

The present investigation focuses on TME activity over the Southern Hemisphere (SH) and attempts to create a climatology of TME events comparable to that found in the Knippertz and Wernli (2010) study. A previous paper by Streten (1973) identified three preferred regions of tropical-midlatitude interaction in the SH. These three regions correspond to the locations of the South Pacific convergence zone (SPCZ; Vincent et al. 1994), the South Atlantic convergence zone (SACZ; Liebmann et al. 1999), and the South Indian convergence zone (SICZ; Cook 2000). Research performed in the current investigation reproduces the location these three convergence zones when identifying the likely preferred pathways of tropical moisture export in the SH.

Information on how these three preferred pathways and individual TME events were identified, as well as where data were obtained, will be presented in the following section. Sections 3a and b will discuss specific findings from the constructed climatology, including the observed intraseasonal and interannual variability in TME frequency within the different pathways. Section 4 highlights the synoptic conditions/dynamic mechanisms associated with

TME events off the Southeast African coast, specifically how seasonal changes in the synoptic pattern may cause the variations in TME frequency observed in Section 3b. This paper will conclude with a brief discussion and presentation of ideas for future research.

2. Data and Methodology

Preferred pathways of poleward moisture transport over the SH were approximated by overlaying seasonally averaged precipitable water (PW) values (mm) and northerly 925-hPa meridional winds ($m\ s^{-1}$) from 1979–2009. These images were created from the 2.5° NCEP–NCAR reanalysis dataset using the General Meteorological Package, GEMPAK (Koch et al. 1983). While moisture flux was not explicitly calculated in this study, the method described above does provide a reasonable first order approximation of the primary locations of poleward moisture transport in the SH.

PW and meridional wind values are the highest, and extended the furthest poleward, in the SH summer months of December, January, and February (DJF). Figure 1 depicts the DJF composite mean of PW (shaded, mm) and northerly 925-hPa meridional winds (dashed contours, $m\ s^{-1}$) from 1979–2009. Similar to the NH, the highest precipitable water values occur on the western edge of the marine subtropical high pressure centers, where anticyclonic circulations redirect warm ocean currents poleward. Overlaying northerly 925-hPa meridional winds on top of the seasonally averaged PW field highlights three regions of inferred poleward moisture transport in the SH, subsequently labeled: (i) the Pacific Ocean (PO) pathway, (ii) the South American (SA) pathway, and (iii) the Southeast African (SEA) pathway.

The PO pathway corresponds to the location of the SPCZ (Vincent et al. 1994). Extending from New Guinea east-southeast toward the central South Pacific, the SPCZ is generally more active in the SH summer months than in the winter months. Similarly, the SA

pathway coincides with the location of the land-based SACZ (Liebmann et al. 1999, Carvalho et al. 2004). Identified as an elongation of convective cloud bands, typically originating over the Amazon River basin and extending over southeastern Brazil, the SACZ is also the most active in the SH summer. The SEA pathway corresponds to the location of the SICZ, discussed extensively by Cook (2000). The SICZ is primarily active in the SH summer when the dominant subtropical high shifts away from the SA coast toward the central Indian Ocean.

A Eulerian PW climatology was constructed to isolate individual TME events within each of the three identified pathways. The climatology identifies grid points along 30°S, every 5° longitude, across three ranges: 175°W to 115°W (PO pathway), 65°W to 20°W (SA pathway), and 35°E to 60°E (SEA pathway). The given ranges were subjectively selected based on the longitudinal extent of the 2 m s^{-1} 925-hPa meridional wind contours and 32 mm PW shading in Figure 1. PW values were extracted four-times-daily from the 2.5° NCEP−NCAR reanalysis dataset for 1979−2007. Only high-end PW values (values at the uppermost extent of each grid point's monthly PW probability density function) were of interest in this study. Potential TME events were identified when two neighboring grid points along 30°S had PW values >93rd percentile of their monthly PW distribution for >24 h. The 93rd percentile nearly approximates 1.5 standard deviations above the mean in a normalized distribution.

Potential events identified in the PW climatology were classified as either "Hits" or "Misses" following human verification of the event's tropospheric structure. TME events, or "Hits," needed to have an elongation of high PW values from the tropics into the midlatitudes, a clear connection to the warm sector of an extratropical cyclone, and occur downstream of a trough axis in the 250-hPa geopotential height field (Fig. 2a,c). The majority of "Misses" were

unstructured blobs of relatively high PW values, displaced far enough poleward to trip the initial PW test (Fig. 2b,d).

3. Results

a) TME detection

Highlighting two neighboring grid points with PW values >93rd percentile of their monthly PW distribution for >24 h lead to the identification of 1113 potential TME events across the three preferred pathways. Of these potential events, 463 met the necessary structural criteria to be classified as "Hits," or TMEs. The probability of detecting a TME event, using this methodology, was 41.6%.

The greatest number of potential TMEs were identified in the PO pathway, with 543 events satisfying the initial PW criteria. Overall, the PO pathway observed the lowest probability of detection of the three analyzed regions (37.2%), with only 202 events meeting the structural parameters necessary to be considered a TME. The same criteria was considerably more successful at identifying TMEs in the SA pathway. Of the 309 possible events identified, 153 were considered "Hits," resulting in a probability of detection of 49.5%. The fewest potential TMEs were associated with the SEA pathway, in which 261 potential events were identified. Of these 261 possibilities, 108 met the structural criteria required to be classified as TME events. The probability of detected a TME in the SEA pathway, using the given methodology, was 41.4%. This percentage is nearly identical to the overall probability of detection found in the study.

b) Interannual and intraseasonal variability

A considerable amount of interannual variability is observed in the frequency of TME events between 1979 and 2007 (Fig. 3a). Year to year fluctuations in frequency appear to be

somewhat consistent between the three pathways from 1979 to 1985. This consistency declines during the late 1980s to early 1990s, when the overall frequency of events observed in the study is at a minimum. Interannual variability in TME frequency is the most pronounced in all three pathways from the mid-1990s to 2007 as TME activity increases. Little to no correlation between the various regions analyzed can be seen during this time period.

Each pathway considered in this analysis experienced at least one TME event per year, based the developed criteria. Ten events was the largest number of TMEs observed in a given year in any of the three pathways. The PO pathway documented ten TME events per year on four separate occasions: 1984, 1995, 2002, and 2007. The SA pathway had nine TME events occur per year in three instances: 1998, 2002, and 2007. Eight events was the yearly maximum observed in the SEA pathway, occurring in 1979 and again in 2006. An interesting point of future research would be to investigate whether TME frequency in any of the analyzed regions was enhanced during these years by the varying phases of ENSO.

Figure 3b illustrates the varying degrees of TME seasonality in the three analyzed regions, depicting event frequency during each month of the year (starting with December). TME events in the PO, represented by the blue line, display the least seasonal variability of the three pathways. An average of seventeen TME events occurred per month over the 29-year period. The SA pathway, denoted by the green line, indicates a season peak in TME activity in the SH summer months of DJF. The number of TMEs observed in DJF (55 events) is more than double the twenty-six events observed in the SH winter months of June, July, and August (JJA). Strong seasonal variability is also associated with TME frequency in the SEA pathway. Forty-six of the 108 confirmed SEA TME events occur in DJF, with only thirteen JJA events during the 29-year period. The SH summer months are ~3.5 times more active than the winter months

in this pathway. A possible cause of this stark seasonal contrast will be discussed in detail in Section 4.

Figure 4a is a composite of the 82 TME events that occurred between November and March during the 29-year climatology. The PW plume associated with TMEs is clearly seen in the composite, extending from the Amazon River basin off the southeast coast of Brazil. This region of high PW values corresponds to the location of the strongest northerly meridional winds at 850-hPa, suggesting that poleward moisture transport was occurring. A cyclonic circulation exists in the 850-hPa vector wind anomaly field at ~50°S. This signature likely represents the circulation around the extratropical cyclones that each TME events was associated with.

Figure 4b depicts a robust TME event that occurred outside the window of this climatology in the SA pathway (and is therefore not a member of the 82 event composite) from 11-16 January 2011. The 1200 UTC 14 January image (created using 0.5° GFS initialized data) looks remarkably like the 82 event composite, to first order. The plume of the highest PW water values coincide with the location of the strongest northerly meridional winds, just of the southeast coast of Brazil. A total of 184.4 mm of rain fell for the city of Teresópolis in Rio de Janeiro, Brazil during the six-day long onslaught of precipitation (INMET, Brazilian National Institute of Meteorology). Over 900 people were killed as a result of flooding and mudslides associated with this TME event.

c) Outliers

There is an obvious decrease in the TME frequency in all three SH pathways during the month of April (Fig. 3b). The authors of this paper have debated the possible causes of this phenomena many times and have come up with few conclusions. One hypothesis is that TMEs simply did not meet the subjective PW criteria as often during April. Varying PW plume widths,

combine with the coarse resolution of the NCEP–NCAR reanalysis dataset, likely caused this climatology to be bias toward identifying TME events with larger longitudinal extensions. The noticeable decrease in TME activity during April remains a point in need of further investigation.

4. Intraseasonal Variability in the SEA Pathway

a) Background

The location of the SEA pathway identified in this study corresponds to a region of persistent cloudiness in the SH, originally documented by Streten (1979). A subsequent paper by Cook (2000) refers to this portion of southern Africa and the southwest Indian Ocean as the South Indian convergence zone (SICZ). Large scale circulations associated with the existence of the SICZ in the SH summer months likely facilitate the creation of an environment favorable for TME development and poleward moisture transport. These features include a persistent low pressure center located over southwestern Africa, an oceanic subtropical anticyclone positioned over the SWIO, and 250-hPa geopotential height trough over southeastern Africa, extending east and to the south of Madagascar (Cook 2000, Todd et al. 2004) (Fig. 5). This portion of the study focuses on TME activity associated with the SEA pathway and the possible contribution of the SICZ to the high frequency of events observed during the region's warm season.

b) Data and Methodology

Composite images of the atmospheric conditions present during the 108 identified SEA TME events are constructed using the NCEP–NCAR reanalysis dataset available through the 'daily mean composites' feature on the NOAA Earth System Research Laboratory (ESRL) website (Kalnay et al. 1996). Comparisons of DJF and JJA sea level pressure (SLP), 850-hPa vector wind, 250-hPa geopotential height, and PW are also constructed for 1979−2007.

c) Results

Composite images of the 108 TME events depict the average atmospheric conditions during which the events occurred (Fig. 6). The composite mean SLP field reveals a pattern consistent with that observed under active SICZ conditions in Cook (2000) and Todd et al. (2004) (Fig. 6a). A relatively weak low pressure center is located over southwestern Africa, corresponding to the region of the highest 925-hPa air temperature values south of the equator (Fig. 6b). The dominant subtropical high pressure center is located at ~32°S and 80°E. Flow around these two features, depicted in the 850-hPa vector wind anomaly field, results in the zonal convergence of air masses at low-levels between Mozambique and the west coast of Madagascar (Fig. 6c). Continued northerly flow along the east African coastline also results in the advection of air that was warmed over central Africa and the tropical Indian Ocean through the combination of sensible and diabatic heating. Low-level convergence and warm air advection, in keeping with the concepts of mass continuity and quasi-geostrophic theory, are associated with forcing for ascent within the column. Negative ω values are depicted in the 108 event composite at 600-hPa (Fig. 6d). Low to mid-level heating and forcing for ascent results in a region of lower SLP off the coast of Mozambique and contributes to the cloudiness and elevated precipitation rates associated with TME events.

Variations in the position of the individual midlatitude cyclones associated with each TME event likely caused the surface low pressure center to be washed out in the 108 event average. However, the signal of an elongated upper-level trough and ridge couplet is evident in the 250-hPa geopotential height field (Fig. 7a). The amplified trough corresponds to a -20 m deviation from the climatological average, while the amplified ridge corresponds to a +80 m

anomaly (Fig. 7b). The region of upper-level divergence downstream of the 250-hPa trough axis is conducive for the development of extratropical cyclones, which by definition are necessary for TME events to occur.

The combination of the large scale flow pattern associated the surface heat low over southwestern Africa and marine subtropical high pressure center above the southern Indian Ocean, coupled with an upper-level flow pattern favorable for the development of extratropical cyclones around 45°S, produces an environment conducive for tropical moisture export. The composite anomaly of 700-hPa moisture flux, associated with the 108 events identified in this 29-year climatology, depicts values exceeding 150 (g kg^{-1})*(m s^{-1}) extending from central Africa, off the southeast coast, into the midlatitudes (Fig. 8b). A zonally confined and meridionally elongated plume of anomalous PW values occurs over the same location, consistent with the structure and definition of a TME event (Fig. 8d).

d) Seasonal synoptic conditions

The composite mean conditions during which the 108 identified SEA TME events occur is nearly identical to the synoptic conditions associated with an active SICZ (Cook 2000, Todd et al. 2004) (Fig. 5). The SICZ is a land-based convergence zone, active almost exclusively in the SH warm season. The large scale circulation changes responsible for the seasonality of the SICZ likely play a major role in the observed intraseasonal variability in TME frequency.

Figure 9 provides a comparison of warm season (DJF) and cool season (JJA) SLP, 850-hPa vector wind, 250-hPa geopotential height, and the PW water field over the SEA pathway from 1979−2007. The heat low over southern Africa and the oceanic high pressure center that exist in DJF facilitate the convergence and poleward flow of 850-hPa winds along western Madagascar (Fig. 9a,c). Wind vectors over this region are nearly reversed in JJA. As the highest

values of incoming solar radiation progress back into the NH, the SH (particularly the African continent) cools (not shown). The continental low pressure center weakens and shifts equatorward, allowing the dominant subtropical high pressure center to shift 30° to the west over South Africa (Fig. 9b). The 250-hPa ridge shifts westward in response, replacing the DJF climatological trough that existed south of Cape Town (Fig. 9f). Low-level flow in this synoptic regime has a southerly component along the east coast of Africa (Fig. 9d).

The JJA reduction in zonal convergence and poleward flow at low-levels, corresponding to the shift in large scale circulation features, causes the highest SH PW values to be confined to the equatorial region (Fig. 9h). PW confinement in the tropics, in conjunction with westward propagation of the favorable region for divergence at 250-hPa, likely results in the seasonality of the SICZ and DJF minimum in TME events observed in the SEA pathway.

4. Discussion and Conclusions

Tropical moisture export (TME) events are important features in the global circulation, linking moisture sources in the tropics to heavy precipitation events in the midlatitudes (Knippertz and Wernli 2010). This study constructs a preliminary 29-year climatology of TMEs in the SH, utilizing the 2.5° NCEP–NCAR reanalysis dataset. Three likely regions of poleward moisture transport were considered in this investigation, labeled: (i) the Pacific Ocean (PO) pathway, (ii) the South American (SA) pathway, and (iii) the Southeast African (SEA) pathway. These three regions correspond to the locations of the South Pacific, South Atlantic, and South Indian convergence zones, respectively.

PO TME events occur in the central South Pacific and exhibit the least seasonal variability of the three examined locations (Fig. 9b). Precipitation associated with TMEs in this region primarily affects the islands of French Polynesia. TMEs that occur in the SA pathway

funnel moisture from the tropical Atlantic and Amazon rainforest over the southeastern coast of Brazil. The frequency of TMEs within this region reaches a seasonal peak in the SH summer.

TME events in the SEA pathway mainly impact Madagascar and the southernmost expanses of the Indian Ocean. The frequency of TMEs off the southeast African coast is ~3.5 times greater in the SH summer months (DJF) than the winter months (JJA). This study suggests that the region's seasonal peak in DJF is likely related to the active phase of the SICZ, when synoptic conditions identified by Cook (2000) and Todd et al. (2004) are more favorable for poleward moisture transport.

Ideally, the preliminary climatology presented here will be expanded upon by a comprehensive trajectory analysis, similar to that performed in the Knippertz and Wernli (2010) study. As written, the current investigation provides a useful basis for the future identification of high-impact sensible weather events in the SH midlatitudes. Unanticipated points of further interest have arisen from this study, including the possible impact of ENSO on the interannual variability of TMEs observed in Figure 3a, as well as the unexpected decrease in TME activity during the month of April across all three examined regions. The authors leave these research questions to future analyses.

Acknowledgements. The results presented in this paper would not have been possible without the help and guidance of many students and faculty members at the Department of Atmospheric and Environmental Sciences at the University at Albany, State University of New York. I particularly wish to thank Dr. Lance Bosart (DAES Distinguished Professor), both for his encouragement and support of my research interests, as well as for the opportunities he provided me with throughout my undergraduate career. I would like to extend special thanks and appreciation to DAES graduate student Jason Cordeira, whose invaluable computer programming assistance and intellectual advice made me a better scientist. I also wish to thank DAES graduate students Heather Archambault, Nicholas Metz, and Alan Srock, as well as Ross Lazear (Instructional Support Specialist) and Kevin Tyle (DAES Systems Administrator), for their assistance computing and preparing presentations of this work. Finally, I wish to thank those individuals who contributed to the thought provoking and intellectual discussion of TMEs on the DAES research (map) e-mail list.

References

Browning, K. A., and C. W. Pardoe, 1973: Structure of low-level jet streams ahead of mid-latitude cold fronts. *Quart. J. Roy. Meteor. Soc.*, **99**, 619– 638.

Carlson, T. N., 1980: Airflow through midlatitude cyclones and the comma cloud pattern. *Mon. Wea. Rev.*, **108**, 1498-1509.

Carvalho, L. M. V., C. Jones, B. Liebmann, 2004: The South Atlantic Convergence Zone: Intensity, Form, Persistence, and Relationships with Intraseasonal to Interannual Activity and Extreme Rainfall. *J. Climate*, **17**, 88–108.

Cook, K. H., 2000: The south Indian convergence zone and interannual rainfall variability over southern Africa. *J. Climate*, **13**, 3789–3804.

Kalnay, E., and Coauthors, 1996: The NCEP/NCAR 40-Year Reanalysis project. *Bull. Amer. Meteor. Soc.*, **77**, 437-471.

Koch, S. E., M. DesJardins, and P. J. Kocin, 1983: An interactive Barnes objective map analysis scheme for use with satellite and conventional data. *J. Climate Appl. Meteor.*, **22,** 1487–1503.

Knippertz, P., and J. E. Martin, 2007: A Pacific moisture conveyor belt and its relationship to a significant precipitation event in the semiarid southwest United States. *Wea. Forecasting*, **22**, 125-144.

———, and H. Wernli, 2010: A lagrangian climatology of tropical moisture exports to the northern hemispheric extratropics. *J. Climate*, **23**, 987-1003.

Liebmann, Brant, G. N. Kiladis, J. A. Marengo, T Ambrizzi, J. D. Glick, 1999: Submonthly Convective Variability over South America and the South Atlantic Convergence Zone. *J. Climate*, **12**, 1877–1891.

Newell, R. E., N. E. Newell, Y. Zhu, and C. Scott, 1992: Tropospheric rivers?—A pilot study. *Geophys. Res. Lett.*, **19**, 2401-2404.

Streten, N. A., 1973: Some characteristics of satellite-observed bands of persistent cloudiness over the Southern Hemisphere. *Mon. Wea. Rev.*, **101,** 486–495.

Todd, M. C., R. Washington, P. L. Palmer, 2004: Water vapour transport associated with tropical-temperate through systems over southern Africa and the southwest Indian Ocean. *Int. J. Climatol.*, **24**, 555-568.

Vincent, D. G., 1994: The South Pacific Convergence Zone (SPCZ): A Review. *Mon. Wea. Rev.*, **122**, 1949-1970.

Zhu, Y., and R. E. Newell, 1994: Atmospheric rivers and bombs. *Geophys. Res. Lett.*, **21**, 1999-2002.

———, and ———, 1998: A proposed algorithm for moisture fluxes from atmospheric rivers. *Mon. Wea. Rev.*, **126**, 725–735.

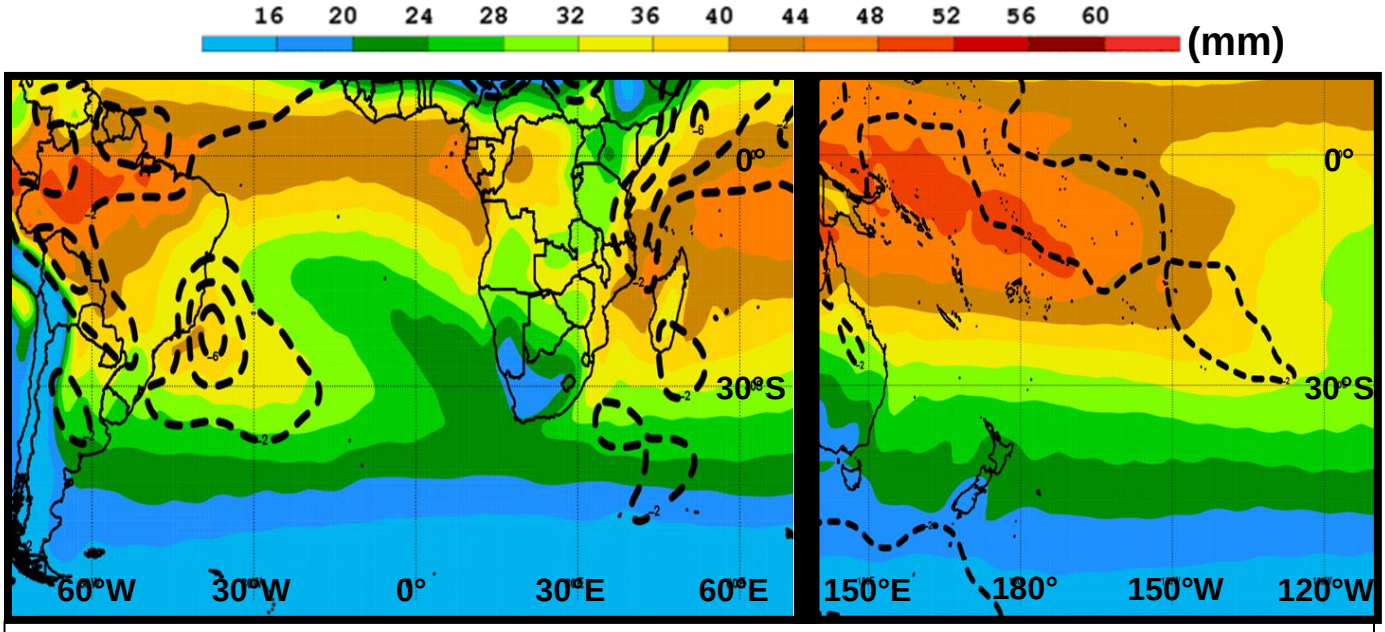

FIG. 1. Composite image of PW (shaded, mm) and northerly 925-hPa meridional winds (dashed contours, m s^{-1}), averaged over DJF of 1979–2009. The highest PW values exist on the western edge of the dominant marine subtropical high pressure centers. These regions of high PW values, coupled with the 2 m s^{-1} northerly meridional wind contour, highlight the locations of the South Atlantic, South Indian, and South Pacific convergence zones (from left to right), originally identified by Streten (1979).

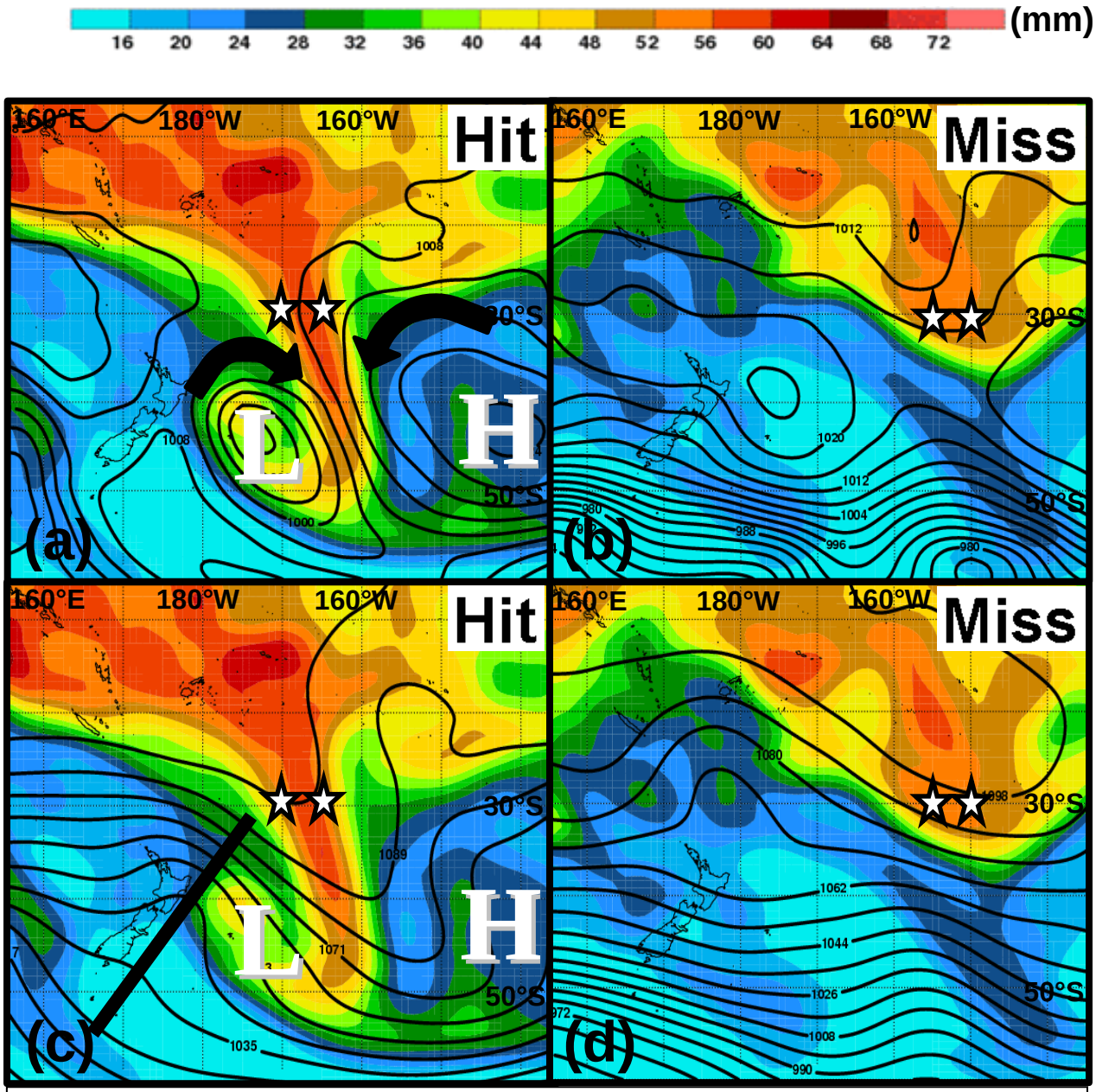

FIG. 2. A human verification process separated potential TME events into two categories, "Hits" and "Misses," based on a specific set of structural criteria. PW (shaded, mm) and SLP (black contours, hPa), are depicted for a: (a) "Hit," or TME event, at 0000 UTC 19 February 1988, and (b) "Miss" at 0000 UTC 4 April 1990. "Hits" contained an elongation of relatively high PW values from the tropics into the midlatitudes in association with the warm sector of an extratropical cyclone. Below, PW (shaded, mm) and 250-hPa geopotential heights (black contours, dam), are depicted for the same: (c) "Hit" and (d) "Miss". Plumes of PW needed to occur downstream of the 250-hPa geopotential height trough axis to be classified as a TME event.

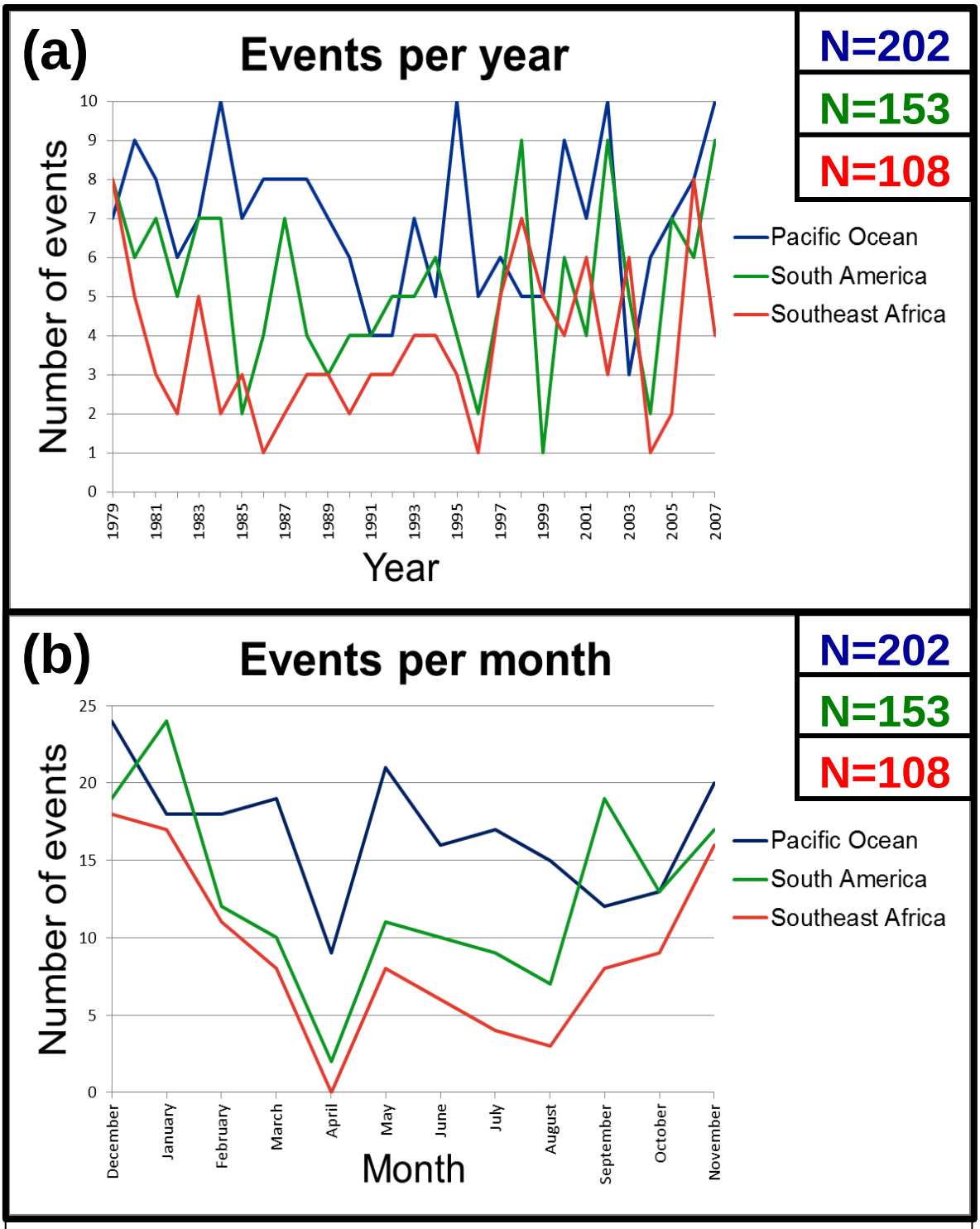

FIG. 3. These graphs represent the frequency of TME events in the PO (blue), SA (green), and SEA (red) pathways, viewed (a) per year and (b) per month. A considerable amount of interannual variability is associated with all three pathways. The PO pathway displays little seasonal variation in TME frequency, while the SA and SEA pathways have pronounced frequency maxima in the SH warm season (DJF).

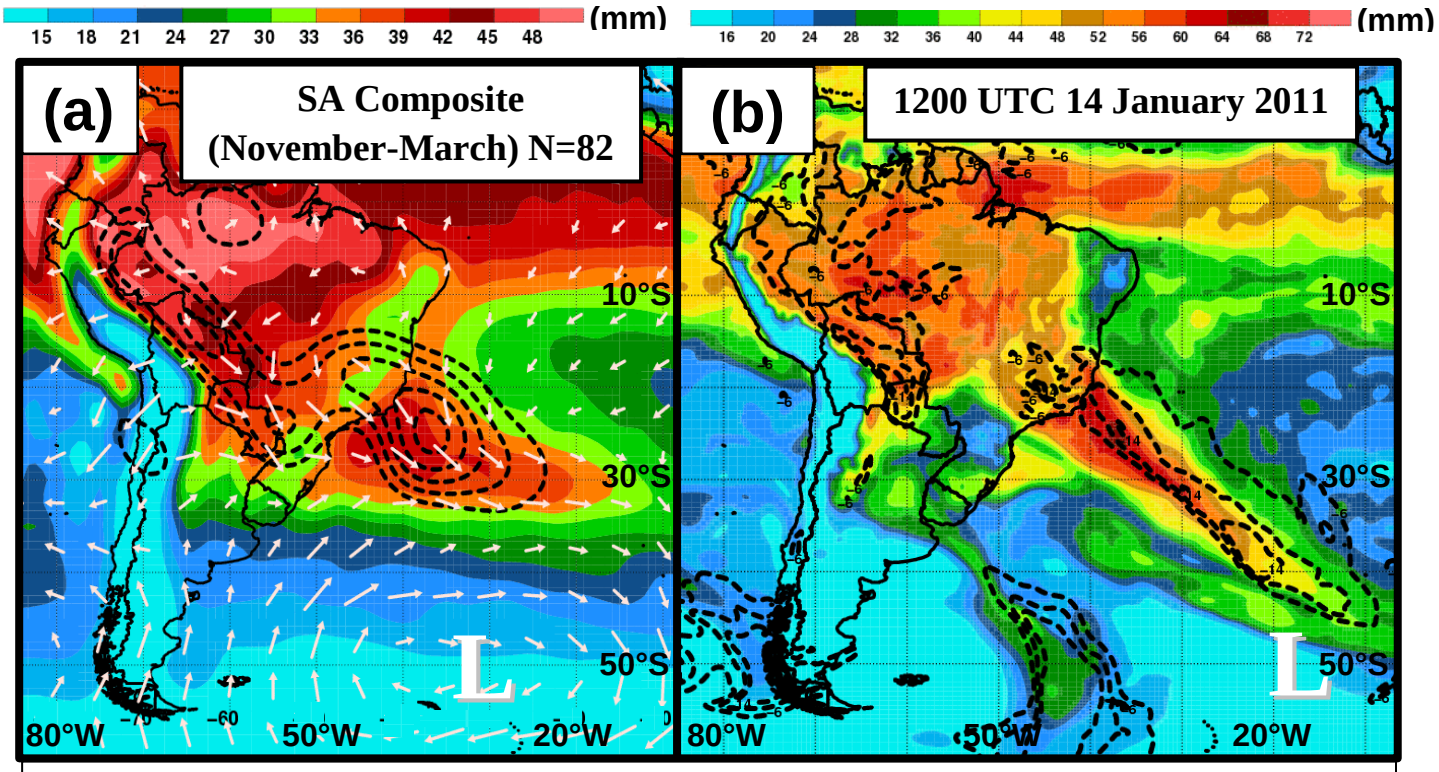

FIG. 4. Figure 4a is a composite image of PW values (shaded, mm), northerly 850-hPa meridional wind (black dashed contours, beginning at -3 m s^{-1}), and the 850-hPa vector wind anomaly (m s^{-1}) for the 82 TME events that occurred in the SA pathway from November-March. Figure 4b depicts PW values (shaded, mm) and northerly 850-hPa meridional wind (black dashed contours, beginning at -6 m s^{-1}) for a high-impact TME event that occurred outside the window of this climatology on 1200 UTC 14 January 2011. The individual TME event exhibits the key characteristics of the 82 event composite, particularly: 1) the plume of high PW off the southeast coast of Brazil, 2) a maximum in northerly meridional winds along the length of the PW plume, and 3) an extratropical cyclone positions over 50°S.

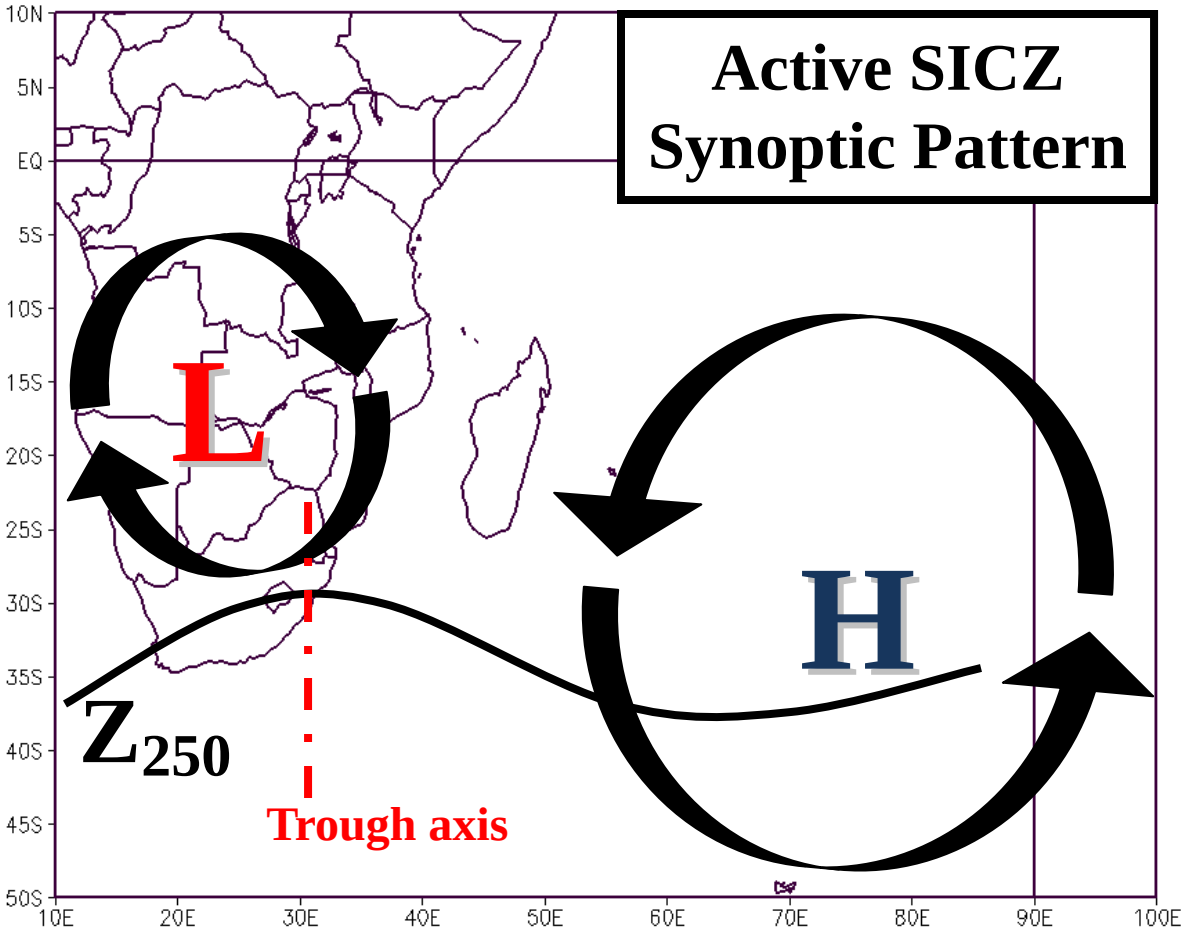

FIG. 5. Schematic representation of the synoptic pattern associated with the active South Indian convergence zone (SICZ) as described by Cook (2000) and Todd et al. (2004).

Map courtesy of: NOAA/ESRL Physical Sciences Division

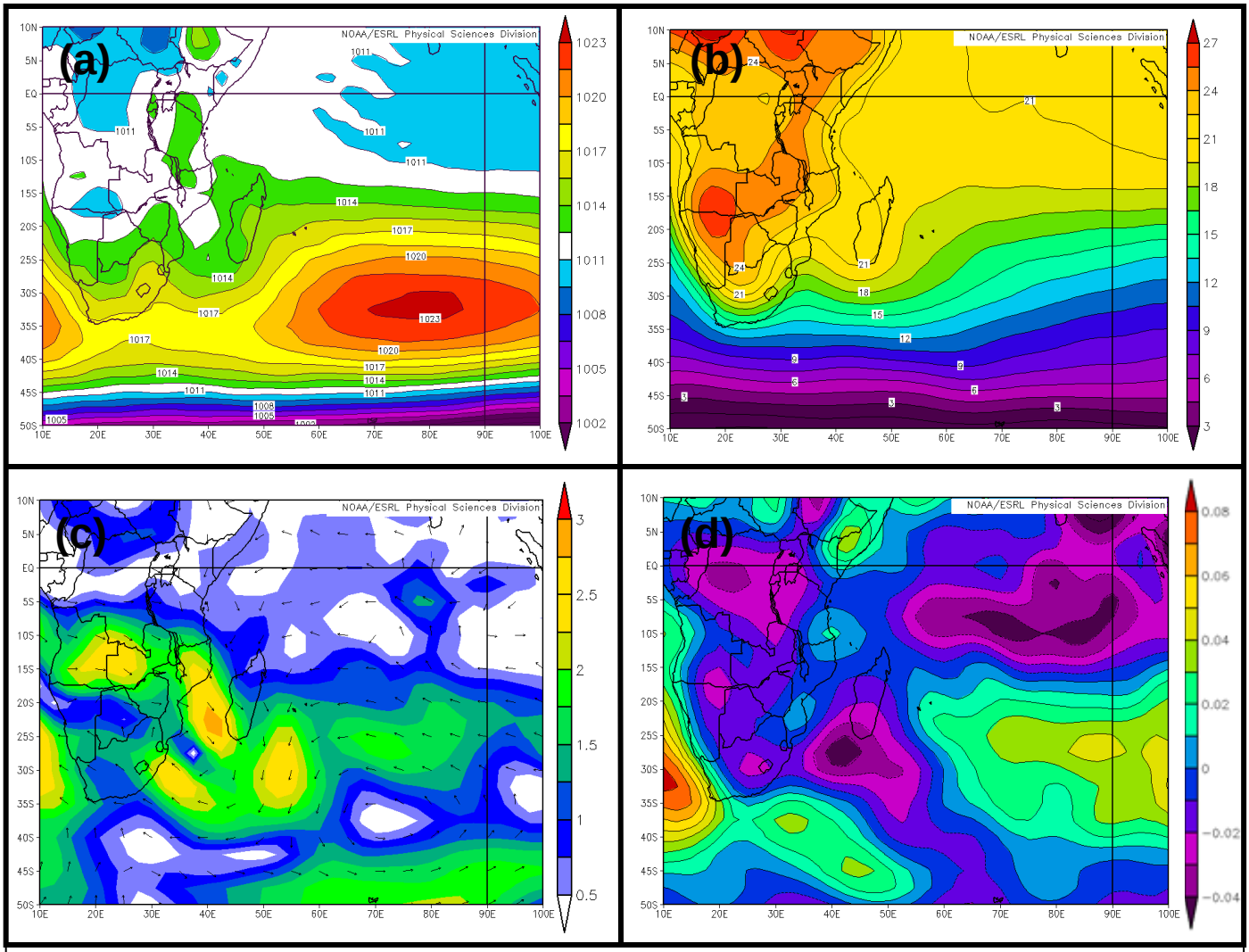

FIG. 6. Composite images of the 108 identified TME events, including: (a) mean sea level pressure (shaded, hPa), (b) 925-hPa air temperature (shaded, °C), (c) 850-hPa vector wind anomaly (vectors with magnitude shaded, m s^{-1}), and (d) omega (shaded, Pa s^{-1}). Large scale features present in the composites are nearly identical to those described by Cook (2000) and Todd et al. (2004) when the South Indian convergence zone is active (Fig. 4). Source: NOAA/ESRL Physical Sciences Division

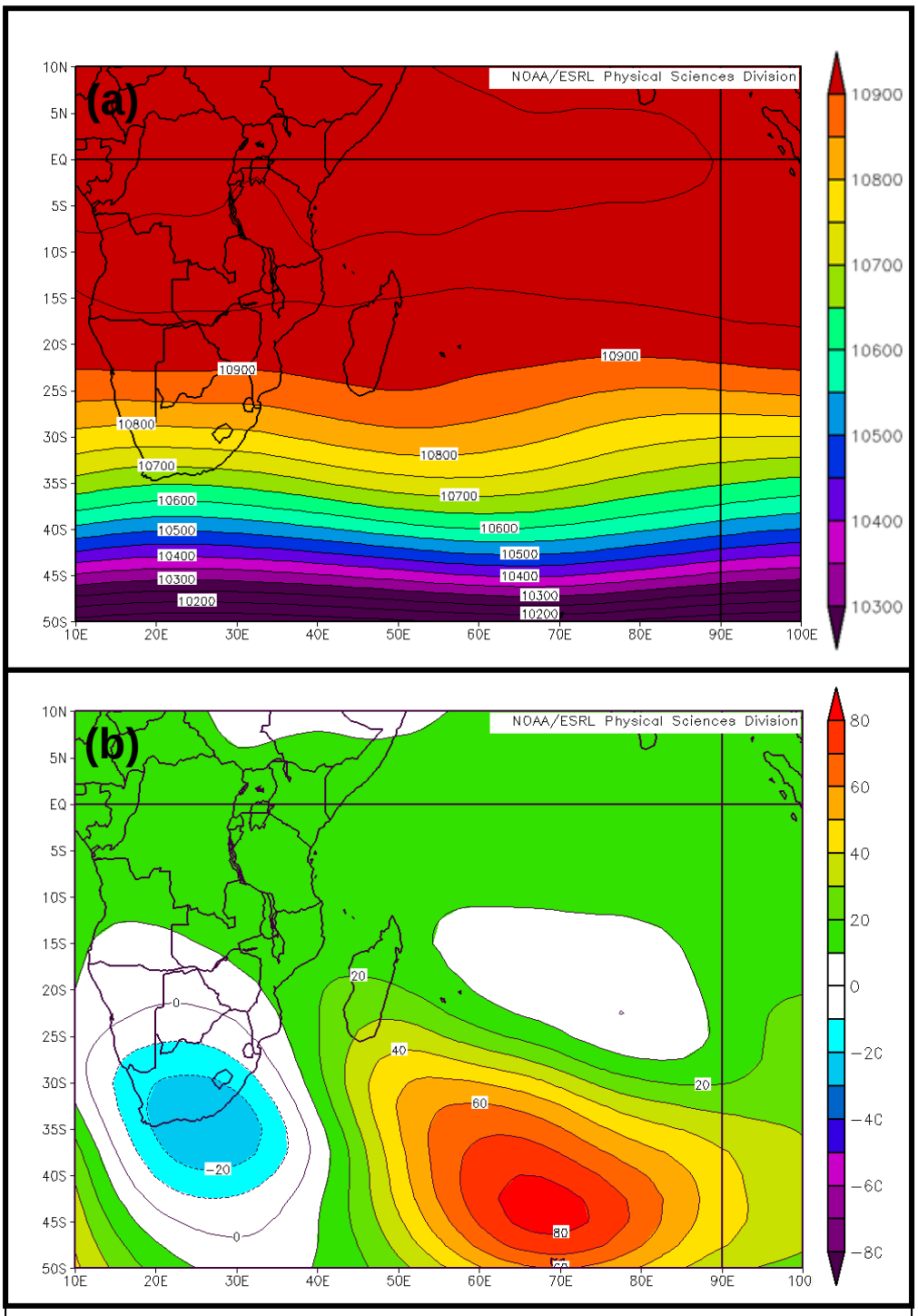

FIG. 7. This image depicts composites of: (a) 250-hPa geopotential height (shaded, m), and (b) 250-hPa geopotential height anomalies (shaded, m) for the 108 TME events identified in the SEA pathway.

Source: NOAA/ESRL Physical Sciences Division

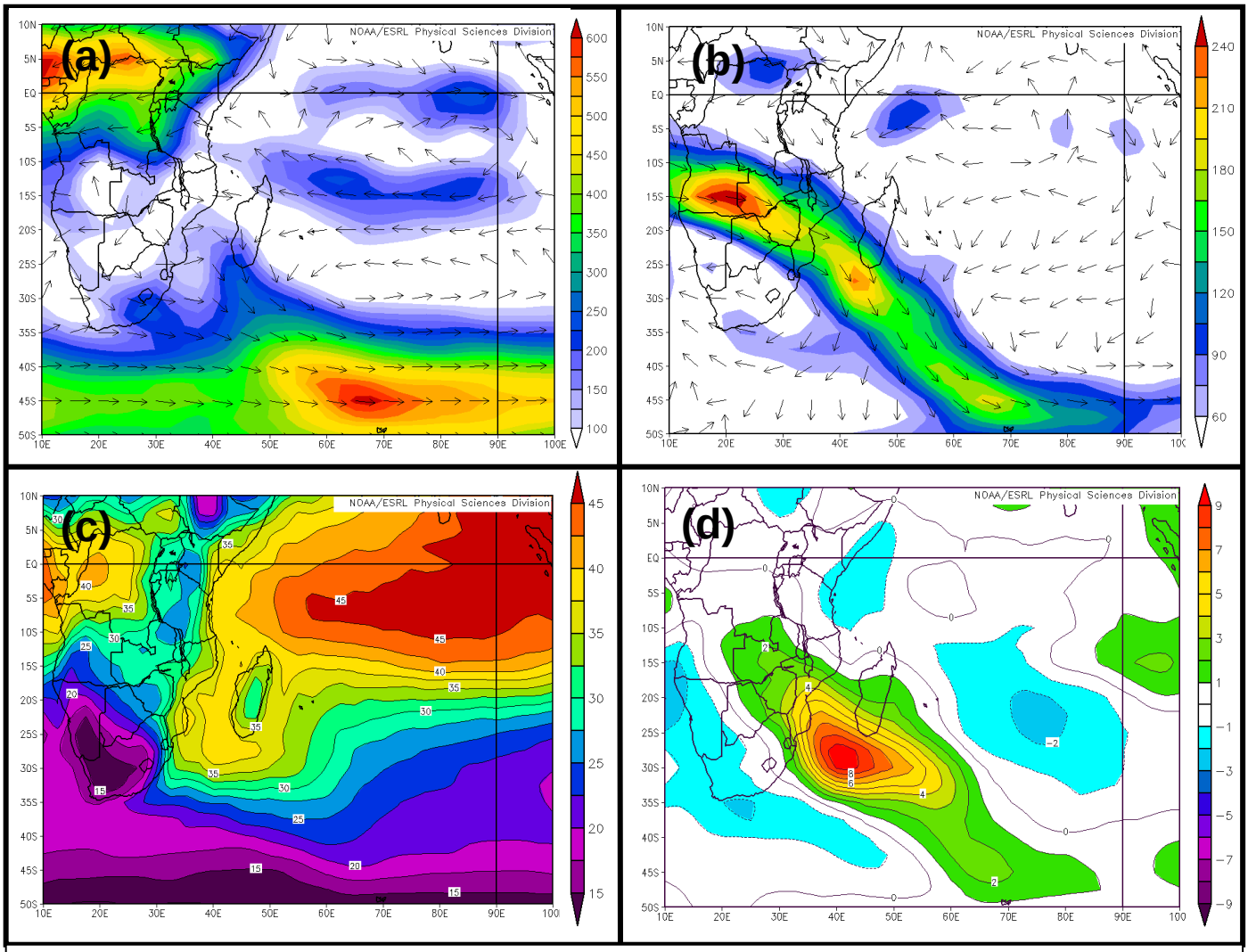

FIG. 8. Composite images of the 108 TME events, including: (a) 700-hPa moisture flux (shaded with vectors, (g kg^{-1})*(m s^{-1})), (b) 700-hPa moisture flux anomaly (shaded with vectors, (g kg^{-1})*(m s^{-1})), (c) PW (shaded, kg m^{-2}), and (d) PW anomaly (shaded, kg m^{-2}). Plumes of high precipitable water values extending poleward off the southeastern portion of Africa is a classic characteristic of TMEs in this region.

Source: NOAA/ESRL Physical Sciences Division

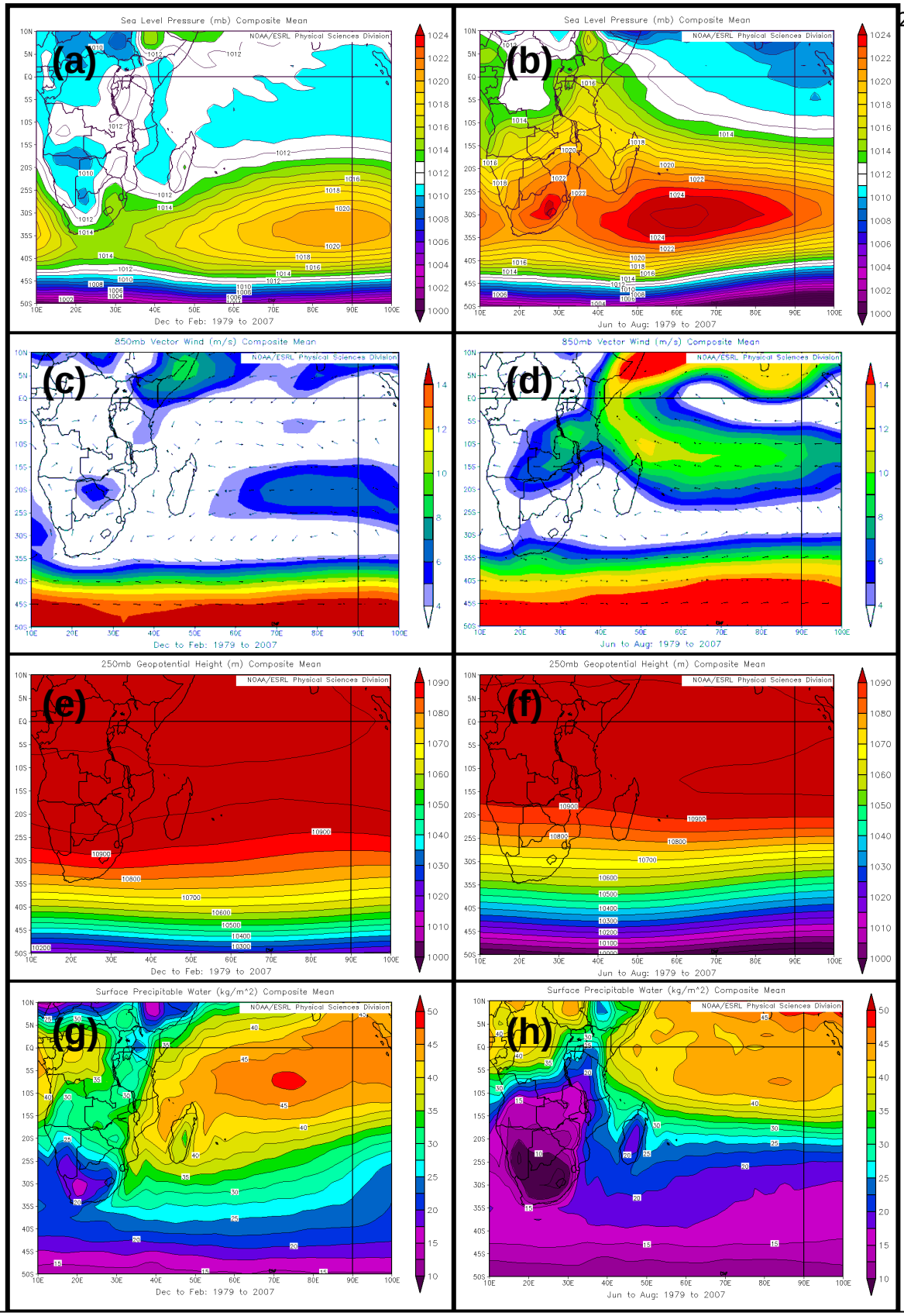

FIG. 9. These images provide a seasonal comparison of the SWIO. Panels include: (a) DJF mean sea level pressure (shaded, hPa), (b) JJA mean sea level pressure (shaded, hPa), (c) DJF 850-hPa vector wind (vectors with magnitude shaded, m s^{-1}), (d) JJA 850-hPa vector wind (vectors with magnitude shaded, m s^{-1}), (e) DJF 250-hPa geopotential height (shaded, m), (f) JJA 250-hPa geopotential height (shaded, m), (g) DJF PW values (shaded, kg m^{-2}), and (h) JJA PW values (shaded, kg m^{-2}). Source: NOAA/ESRL Physical Sciences Division